


[View Journal Online](#)
[View Article Online](#)

Synthesis, computational studies, and Hirshfeld surface analysis of 2H-chromen-2-one and imine derivatives

Felix Odame ^{1,*}, Tatenda Madanhire ², Jerry Joe Ebo Kingsley Harrison ³, Nathaniel Owusu Boadi ⁴ and Eric Hosten ²

¹ Department of Basic Sciences, School of Basics and Biomedical Sciences, University of Health and Allied Sciences, PMB 31, Ho, Ghana

² Department of Chemistry, Nelson Mandela University, PO Box 77000, Gqeberha 6000, South Africa


³ Department of Chemistry, University of Ghana, PO Box LG 56, Legon, Accra, Ghana

⁴ Department of Chemistry, Kwame Nkrumah University of Science and Technology, Kumasi, University Post Office, Kumasi, Ghana

* Corresponding author at: Department of Basic Sciences, School of Basics and Biomedical Sciences, University of Health and Allied Sciences, PMB 31, Ho, Ghana. e-mail: fodame@uhas.edu.gh (F. Odame).

RESEARCH ARTICLE



 10.5155/eurjchem.14.2.287-296.2389

Received: 18 December 2022

Received in revised form: 06 March 2023

Accepted: 26 March 2023

Published online: 30 June 2023

Printed: 30 June 2023

KEYWORDS

Imine
 Crystal
 Coumarin
 Monoclinic
 Chemical reactivity
 Hirshfeld surface analysis

ABSTRACT

Some 2H-chromen-2-one and imine derivatives have been synthesized through a one-pot condensation of aldehydes, diethyl malonate, and amine compounds. The compounds obtained have been characterized using FTIR, NMR, GC-MS, and elemental analysis. The single-crystal X-ray structure of 3-[piperidine-1-carbonyl]-2H-chromen-2-one (2) has been presented. Compound 2, recrystallized in the monoclinic space *C2/c* (no. 15), *a* = 16.654(15) Å, *b* = 8.789(7) Å, *c* = 18.460(18) Å, β = 102.89(5)°, *V* = 2634(4) Å³, *Z* = 8, *T* = 296(2) K, $\mu(\text{MoK}\alpha)$ = 0.091 mm⁻¹, *D*_{calc} = 1.298 g/cm³, 17626 reflections measured (4.528° ≤ 2 θ ≤ 57.446°), 3321 unique (*R*_{int} = 0.0313, *R*_{sigma} = 0.0257) which were used in all calculations. The final *R*₁ was 0.0441 (*I* > 2 σ (*I*)) and *wR*₂ was 0.1329 (all data). The experimental bond lengths, bond angles, and other topological properties of compound 2 were compared with the DFT calculated results, the comparison showed good agreement with each other with varying level deviations. The energy levels of HOMO and LUMO, as well as the global chemical reactivity descriptors of representative compound 2, have been presented. A discussion of the Hirshfeld surface analysis of compound 2 has been carried out to provide insight into its structural properties.

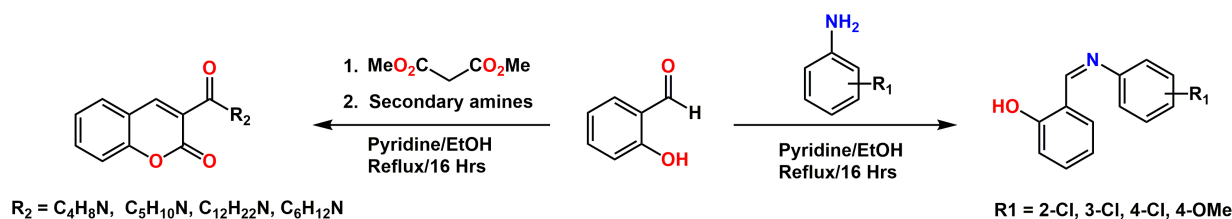
Cite this: *Eur. J. Chem.* 2023, 14(2), 287-296

Journal website: www.eurjchem.com

1. Introduction

Syntheses of some ethyl coumarin-3-carboxylate and other derivatives of coumarin have been described [1-14]. Coumarinyl-1,4-benzodioxanes were accessed by the reaction between a variety of 2-[[*o*-iodophenoxy)methyl]oxiranes and some hydroxycoumarin isomers using CuI and 1,10-phenanthroline as catalysts. The compounds showed significant free hydroxyl radical scavenging activity [2]. Some hydroxyl-coumarin compounds have been prepared by the reaction of hydroquinone with ethylacetoacetate and aniline derivatives. The compounds exhibited moderate to high antioxidant activity [3]. Different coumarin derivatives have been synthesized using 4-bromomethylcoumarins and their sulphonyl chlorides, while some benzofuran derivatives have been accessed through ethyl 3-(bromomethyl)-6-methoxy-1-benzofuran-2-carboxylate and different imidazoles and their benzo analogues [4]. A variety of coumarin hydrazides have been synthesized by the reaction of 1H-benzotriazole derivatives with nicotinic hydrazide, benzo-hydrazide, and phenyl acetic hydrazide. The compounds showed good antioxidant and antilipase activities [5]. The

condensation reaction between ethyl acetoacetate and resorcinol has been used to synthesize some coumarin derivatives. The compounds exhibited good antioxidant, analgesic, and anti-inflammatory activities [6]. The use of the Knoevenagel condensation technique to synthesize some coumarin derivatives has been reported, with hydrazine and thiazole being incorporated into the compounds. The compounds have been reported to exhibit low toxicity against human periodontal ligament fibroblast cells (HPDLF) [7]. The synthesis of some 4-hydroxycoumarin derivatives was achieved by the reaction of 2-acetoxy benzoyl chloride with ethyl acetoacetate. The compounds exhibited good antibacterial and antifungal activities [8]. Some coumarin compounds have been studied for their fluorescent properties. The compounds were found to allow the imaging of human neuroblastoma SH-SY5Y cell membranes [9]. Carbonitriles and derivatives of pyrazole coumarin have been synthesized by multistep synthesis using 3-acetyl-4-hydroxycoumarin as the starting material. The compounds showed good antibacterial activity, but weak to moderate cytotoxicity against human breast adenocarcinoma and hepatocarcinoma cell lines [10].



Scheme 1. Synthesis of 3-[piperidine-1-carbonyl]-2H-chromen-2-one and imine derivatives.

The synthesis of 1,2,3-triazole-linked coumarins has been achieved *via* click chemistry. The compounds exhibited good antibacterial activity which was collaborated by *in silico* docking studies [11]. Some coumarin hydrazones and amide derivatives have been synthesized through multistep synthesis. The compounds showed good antibacterial activity against *Staphylococcus aureus*, *Streptococcus pneumoniae*, *Escherichia coli*, and *Pseudomonas aeruginosa* [12]. Some coumarin derivatives with fungicidal activity have been synthesized through cyclization and condensation reactions using resorcinol and substituted β -keto esters as starting materials [13]. Some thiazolyl coumarin derivatives have been synthesized by one-pot condensation of 3-acetyl-4-hydroxycoumarin, aryl aldehydes, thiourea, and ammonium acetate [14]. Most of the reported methods for synthesizing coumarins involve multistep synthesis. In this work, we set out to develop a one-pot method of synthesizing coumarins that could be used in accessing different coumarins derivatives for various applications.

This study reports the synthesis, characterization, and computational studies of some chromen-2-one and imine derivatives. A discussion on single-crystal XRD analysis of 3-[piperidine-1-carbonyl]-2H-chromen-2-one (**2**) has been presented to provide insight into the structural properties of the compounds. The theoretical bond lengths and bond angles of compound **2** have been compared with the experimental data. The Hirshfeld surface analysis, HOMO-LUMO, and chemical reactivity descriptors have also been computed and discussed.

2. Experimental

2.1. Reagents and instrumentation

Analytical grade reagents and solvents for synthesis such as salicylaldehyde, pyrrolidine, piperidine, and ethyl acetoacetate were obtained from Sigma-Aldrich, USA, while ethanol, diethyl ether, and pyridine were obtained from Merck Chemicals, South Africa. The chemicals were used as received (*i.e.*, without further purification). The 1H NMR and ^{13}C NMR spectra were recorded on a Bruker Avance AV 400 MHz spectrometer operating at 400 MHz for 1H and 100 MHz for ^{13}C using DMSO- d_6 as solvent and tetramethylsilane as the internal standard. Chemical shifts are expressed in ppm. FTIR spectra were recorded on a Bruker Platinum ATR Spectrophotometer Tensor 27. Elemental analyses were performed using a Vario Elementar Microcube ELIII. Melting points were obtained using a Stuart SMP30 while the masses were determined using an Agilent 7890A GC system connected to a 5975C VL-MS-C with electron impact as the ionization mode and detection by a triple-axis detector. The GC was fitted with a 30 m \times 0.25 mm \times 0.25 μ m DB-5 capillary column. Helium was used as a carrier gas at a flow rate of 1.63 mL/min with an average velocity of 30.16 cm/s and a pressure of 63.73 kPa.

2.2. X-ray crystallographic measurements

X-ray diffraction analysis of compound **2** was performed at 200 K using a Bruker Kappa Apex II diffractometer with mono-

chromated MoK α radiation ($\lambda = 0.71073$ Å). APEXII [15] was used for data collection and SAINT software [16] for cell refinement and data reduction. The structures were solved by direct methods using SHELXS-2013 [15] and refined using least squares procedures using SHELXL-2013 [16] with SHELXLE [17] as a graphical interface. All non-H atoms were refined anisotropically. Carbon-bound H atoms were placed in calculated positions (C-H = 0.95 Å for aromatic carbon atoms and C-H = 0.99 Å for methylene groups) and were included in the refinement in the riding model approximation, with U_{iso} (H) set to 1.2 U_{eq} (C). The H atoms of the methyl groups were allowed to rotate with a fixed angle around the C-C bond to best fit the experimental electron density (HFIX 137 in the SHELX program suite [16]) with U_{iso} (H) set to 1.5 U_{eq} (C). Nitrogen-bound H atoms were located on the Fourier map and freely refined. Data were corrected for absorption effects using the numerical method implemented in SADABS [17-20]. The molecular graphics were performed using ORTEP-3 [21], while the materials for publication were prepared using Mercury [22] and PLATON [23].

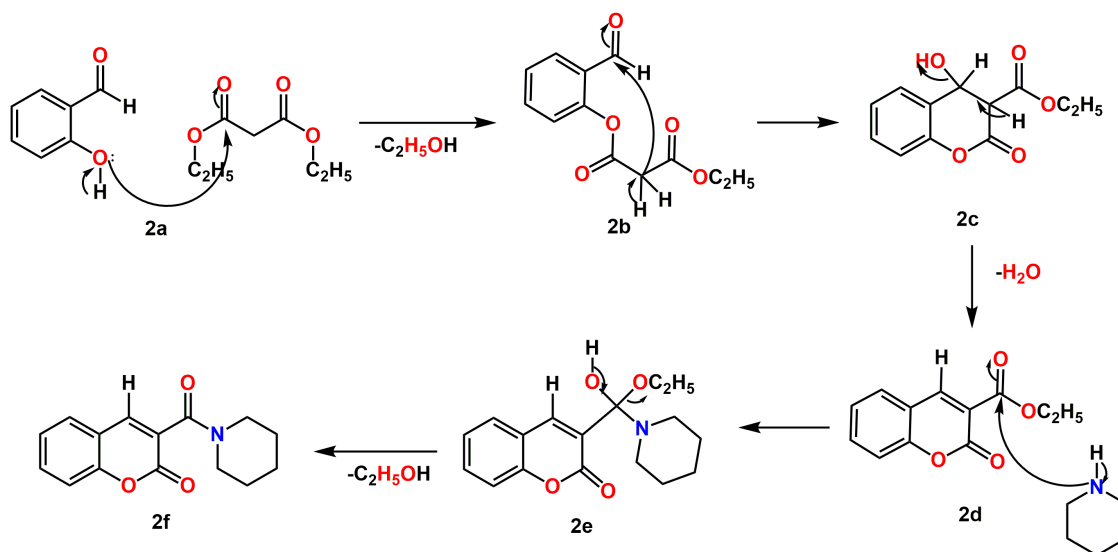
2.3. Computational studies

The calculations were carried out using the Gaussian 09 program [24]. Molecular geometries of the singlet ground state of all compounds were fully optimized in the gas phase at the density functional theory (DFT) using the B3LYP [25], CAM-B3LYP [26], B3PW91 [27], wB97XD [28] and M06 functionals [29] and the 6-311G(d,p) basis set [30]. Different functionals and basis sets were used to determine the functional that gives the values most consistent with the experimental values or the functionals that best describes the experimental values. The structures were optimized and subjected to frequency calculations to ensure that the optimized molecular structures corresponded to a minimum. The results were viewed in Avogadro [31] or Gauss View 6.0 [32]. Frequency optimization of the structures was done using the Gaussian 09 program [24].

2.4. General method for the synthesis of compounds 1-7

Different amines (aromatic and cyclic amines) (0.02 mol) were dissolved in a minimal amount of ethanol and treated with four drops of pyridine and placed in a round bottom flask. Salicylaldehyde (0.02 mol, 2.44 g) and diethyl malonate (0.02 mol, 3.20 g) were dissolved in ethanol, added to the mixture, and heated under reflux for 16 h. The reaction mixture was allowed to stand overnight in a fumehood and the precipitate that was collected was recrystallized in ethanol: diethyl ether (1:1, v:v) (Scheme 1).

3-(Pyrrolidine-1-carbonyl)-2H-chromen-2-one (1): Color: Light brown. Yield: 79%. M.p.: 124-126 °C. FT-IR (ATR, v, cm $^{-1}$): 2969 (C-H), 2875 (C-H), 1781 (C=O) (amide), 1612 (C=C), 1569 (C=C), 1460 (C-N), 1421 (C-N). 1H NMR (400 MHz, DMSO- d_6 , δ , ppm): 8.23 (s, 1H, Ar-H), 7.79 (d, 1H, $J = 7.2$ Hz, Ar-H), 7.67 (t, $J = 6.8, 7.6$ Hz, 1H, Ar-H), 7.46 (d, $J = 8.4$ Hz, 1H, Ar-H), 7.40 (t, $J = 6.8, 7.6$ Hz, 1H, Ar-H), 3.44 (s, 2H, CH $_2$ -N), 3.36 (s, 2H, CH $_2$ -N), 1.85 (s, 4H, -CH $_2$ CH $_2$ -). ^{13}C NMR (ppm): 162.9 (C=O), 158.1 (C), 154.1 (C), 142.9 (CH), 133.3 (CH), 129.6 (CH), 126.0 (C), 125.3



Scheme 2. Proposed reaction mechanism for the synthesis of chromen-2-one derivatives.

(CH), 118.7 (C), 116.7 (CH), 47.5 (CH₂), 46.3 (CH₂), 26.0 (CH₂), 24.3 (CH₂). GC-MS (*m/z*) found for C₁₄H₁₃NO₃ = 243.21, calculated mass = 243.26. Anal. calcd. for C₁₄H₁₃NO₃: C, 69.12; H, 5.39; N, 5.76; Found: C, 69.06; H, 5.35; N, 5.71%.

3-[Piperidine-1-carbonyl]-2H-chromen-2-one (2): Color: White. Yield: 81%. M.p.: 191-192 °C. FT-IR (ATR, *v*, cm⁻¹): 3003 (C-H), 2980 (C-H), 1711 (C=O), 1559 (C=C), 1462 (C-N). ¹H NMR (400 MHz, DMSO-*d*₆, *δ*, ppm): 8.16 (s, 1H, Ar-H), 7.78 (d, *J* = 7.6 Hz, 1H, Ar-H), 7.67 (t, *J* = 7.6, 8 Hz, 1H, Ar-H), 7.46 (t, *J* = 8 Hz, 1H, Ar-H), 7.40 (t, *J* = 7.2-7.6 Hz, 1H, Ar-H), 2.09 (s, 2H, CH₂-N), 1.61 (m, 2H, CH₂-N), 1.54 (m, 4H, CH₂-CH₂), 1.49 (m, 2H, CH₂). ¹³C NMR (100 MHz, DMSO-*d*₆, *δ*, ppm): 162.97 (C=O), 157.6 (C), 153.0 (C), 140.6 (CH), 135.2 (CH), 131.3 (CH), 126.7 (C), 120.8 (C), 119.2 (CH), 116.7 (C), 47.8 (CH₂), 42.4 (CH₂), 26.5 (CH₂), 25.8 (CH₂), 24.3 (CH₂). GC-MS (*m/z*) found for C₁₅H₁₅NO₃ = 257.23, calculated mass = 257.28. Anal. calcd. for C₁₅H₁₅NO₃: C, 70.02; H, 5.88; N, 5.44; Found: C, 70.12; H, 5.92; N, 5.48%.

***N,N*-Dicyclohexyl-2-oxo-2H-chromene-3-carboxamide (3):** Color: White. Yield: 51%. M.p.: 176-178 °C. FT-IR (ATR, *v*, cm⁻¹): 3696 (O-H), 2995 (C-H), 2863 (C-H), 2710, 2516, 1764 (C=O), 1650 (C=O), 1605 (C=C), 1481 (C-N). ¹H NMR (400 MHz, DMSO-*d*₆, *δ*, ppm): 8.46 (s, 1H, Ar-H), 7.56 (q, *J* = 8.4-9.2 Hz, 1H, Ar-H), 7.29 (q, *J* = 7.2-8.4 Hz, 2H, Ar-H), 7.19 (s, 1H, Ar-H), 4.35 (q, 2H, CH-N), 1.62 (m, 12H, -CH₂CH₂-), 1.35 (m, 4H, -CH₂CH₂-), 1.19 (m, 4H, -CH₂CH₂-). ¹³C NMR (100 MHz, DMSO-*d*₆, *δ*, ppm): 148.6 (CH), 134.4 (CH), 129.6 (CH), 124.8 (CH), 116.9 (CH), 62.0 (CH₂), 14.3 (CH₂). GC-MS (*m/z*) found for C₂₂H₂₇NO₃: 353.39, calculated mass = 353.45. Anal. calcd. for C₂₂H₂₇NO₃: C, 74.76; H, 7.70; N, 3.96; Found: C, 74.71; H, 7.64; N, 3.91%.

(*E*)-2-(((4-Chlorophenyl)imino)methyl)phenol (4): Color: Yellow. Yield: 80%. M.p.: 99-101 °C. FT-IR (ATR, *v*, cm⁻¹): 2981 (C-H), 1608 (C=N), 1585 (C=C), 1565 (C=C), 1483 (C-N), 1456 (C-N). ¹H NMR (400 MHz, DMSO-*d*₆, *δ*, ppm): 12.83 (s, 1H, OH), 8.54 (s, 1H, N=CH), 7.65 (d, *J* = 6.8 Hz, 1H, Ar-H), 7.49 (d, *J* = 8 Hz, 2H, Ar-H), 7.44 (d, *J* = 6.8 Hz, 3H, Ar-H), 6.98 (d, *J* = 8 Hz, 2H, Ar-H). ¹³C NMR (100 MHz, DMSO-*d*₆, *δ*, ppm): 164.4 (C=N), 160.7 (C), 148 (C), 134.0 (CH), 133.0 (CH), 131.6 (C), 129.8 (CH), 123.6 (CH), 119.8 (CH), 117.1 (CH). GC-MS (*m/z*) found for C₁₃H₁₀ClNO = 231.63, calculated mass = 231.68. Anal. calcd. for C₁₃H₁₀ClNO: C, 67.39; H, 4.35; N, 6.05; Found: C, 67.34; H, 4.32; N, 6.01%.

(*E*)-2-(((3-Chlorophenyl)imino)methyl)phenol (5): Color: Yellow. Yield: 78%. M.p.: 59-61 °C. FT-IR (ATR, *v*, cm⁻¹): 2714 (C-H), 1612 (C=N), 1561 (C=C), 1464 (C-N), 1371 (C-O), 1277 (C-O). ¹H NMR (400 MHz, DMSO-*d*₆, *δ*, ppm): 13.12 (s, 1H, OH),

9.01 (s, 1H, N=CH), 7.70 (d, *J* = 7.2 Hz, 1H, Ar-H), 7.60 (m, 2H, Ar-H), 7.46 (m, 2H, Ar-H), 7.33 (t, *J* = 6.8-7.6 Hz, 1H, Ar-H), 7.01 (d, *J* = 8.0 Hz, 2H, Ar-H). ¹³C NMR (100 MHz, DMSO-*d*₆, *δ*, ppm): 164.9 (C=N), 161.0 (C), 145.2 (C), 134.3 (CH), 133.5 (CH), 130.4 (CH), 128.9 (CH), 128.8 (CH), 128.7 (C), 120.6 (CH), 119.8 (CH), 119.6, 117.7. GC-MS (*m/z*) found for C₁₃H₁₀ClNO = 231.61, calculated mass = 231.68. Anal. calcd. for C₁₃H₁₀ClNO: C, 67.39; H, 4.35; N, 6.05; Found: C, 67.32; H, 4.30; N, 6.00%.

(*E*)-2-(((2-Chlorophenyl)imino)methyl)phenol (6): Color: Yellow. Yield: 81%. M.p.: 65-66 °C. FT-IR (ATR, *v*, cm⁻¹): 3120 (N-H), 2999 (C-H), 1624 (C=N), 1599 (C=C), 1465 (C-N), 1402 (C-N). ¹H NMR (400 MHz, DMSO-*d*₆, *δ*, ppm): 13.12 (s, 1H, OH), 9.02 (s, 1H, N=CH), 7.68 (d, *J* = 7.2 Hz, 1H, Ar-H), 7.60 (m, 2H, Ar-H), 7.46 (m, 2H, Ar-H), 7.33 (t, *J* = 6.8, 7.6 Hz, 1H, Ar-H), 7.01 (d, *J* = 8 Hz, 2H, Ar-H). ¹³C NMR (100 MHz, DMSO-*d*₆, *δ*, ppm): 165.1 (C=N), 161.0 (C), 145.2 (C), 134.3 (CH), 133.4 (CH), 130.3 (CH), 128.9 (C), 128.9 (CH), 128.7 (CH), 120.5 (CH), 119.7 (CH), 117.2 (CH). GC-MS (*m/z*) found for C₁₃H₁₀ClNO = 231.62, calculated mass = 231.68. Anal. calcd. for C₁₃H₁₀ClNO: C, 67.39; H, 4.35; N, 6.05; Found: C, 67.31; H, 4.32; N, 6.00%.

***N*-(4-Methoxyphenyl)-2-oxo-2H-chromene-3-carboxamide (7):** Color: Green solid. Yield: 79%. M.p.: 79-80 °C. FT-IR (ATR, *v*, cm⁻¹): 2964 (C-H), 1743 (C=O), 1549 (C=C), 1363 (C-O). ¹H NMR (400 MHz, DMSO-*d*₆, *δ*, ppm): 13.32 (s, 1H, OH), 8.93 (s, 1H, N=CH), 7.61 (d, *J* = 7.6 Hz, 1H, Ar-H), 7.41 (q, *J* = 8.0-8.8 Hz, 3H, Ar-H), 7.03 (d, *J* = 8 Hz, 2H, Ar-H), 6.97 (d, *J* = 7.28 Hz, 2H, Ar-H), 3.79 (s, 3H, CH₃). ¹³C NMR (100 MHz, DMSO-*d*₆, *δ*, ppm): 161.7 (C=N), 160.7 (C), 159.0 (C), 141.2 (C), 133.2 (CH), 132.7 (CH), 123.1 (CH), 119.9 (C), 119.5 (CH), 117.0 (CH), 115.1 (CH), 55.9 (CH₃). GC-MS (*m/z*) found for C₁₄H₁₃NO₂ = 227.21, calculated mass = 227.26. Anal. calcd. for C₁₄H₁₃NO₂: C, 73.99; H, 5.77; N, 6.16; Found: C, 73.95; H, 5.74; N, 6.12%.

3. Results and discussion

3.1. Synthesis and reaction mechanism

The products were obtained by heating equimolar amounts of the reagents in ethanol for 16 h under reflux. **Scheme 1** shows the synthesis of chromen-2-one and imine derivatives. **Scheme 2** provides a proposed reaction mechanism for the synthesis of 3-[piperidine-1-carbonyl]-2H-chromen-2-one. The reaction is thought to proceed by the abstraction of a proton from the hydroxyl of salicylaldehyde by pyridine in compound **2a** to form the pyridinium ion and a phenoxide that then attacks a

carbonyl on diethyl malonate, leading to the loss of an ethoxide which recovers a proton from the pyridinium ion to give ethanol and pyridine. This leads to the formation of the ethyl-(2-formylphenyl)malonate in compound **2b**. A further abstraction of an acidic proton from the malonate moiety yields a carbanion that attacks the carbonyl of the salicylaldehyde portion of the molecule as indicated in compound **2b** to give an ethyl-4-hydroxy-2-oxochroman-3-carboxylate (**2c**). The abstraction of another acidic proton leads to the formation of a double bond and the loss of a water molecule to give an ethyl-2-oxo-2H-chromene-3-carboxylate in compound **2d**. The deprotonation of piperidine allows the piperidin-1-ide ion formed to attack the carbonyl of ethyl 2-oxo-2H-chromene-3-carboxylate in compound **2d**, which forms 3-(ethoxy(hydroxy)(piperidin-1-yl)methyl)-2H-chromen-2-one in compound **2e**. The loss of an ethanol molecule and the formation of a carbonyl from the hydroxyl lead to the formation of the final product in compound **2f**.

3.2. Spectroscopic characterization

The IR spectrum of compound **1** showed the presence of characteristic absorption peaks at 2969 and 2875 cm^{-1} for the aliphatic C-H stretch. Peaks were observed at 1781, 1612, 1569, and 1460 cm^{-1} for the C=O, C=N, C=C, and C-N absorptions, respectively. The ^1H NMR spectrum indicated the formation of five methylene (CH_2) groups at signals δ 3.44 (2H), 3.36 (2H) and 1.85 (4H) ppm, confirming the incorporation of the pyrrolidine moiety into the compound. The latter was confirmed by ^{13}C NMR and DEPT spectra which showed peaks at 47.5 (CH_2), 46.3 (CH_2), 26.0 (CH_2), and 24.3 (CH_2) ppm. The presence of C=O was determined by a signal at δ 162.9 ppm in the ^{13}C NMR spectrum.

The ^1H NMR spectrum of compound **2** indicated the formation of five sets of methylene protons at δ 2.09, 1.61, 1.54 and 1.49 ppm, confirming the incorporation of the piperidine moiety into the compound. ^{13}C and DEPT spectra also confirmed the incorporation of five methylene (CH_2) groups at δ 47.81, 42.45, 26.51, 25.81 and 24.29 ppm. The IR spectrum of 3-[piperidine-1-carbonyl]-2H-chromen-2-one showed the presence of characteristic absorption peaks at 3003 and 2980 cm^{-1} for the aliphatic C-H stretch, while peaks were observed at 1711, 1636, 1559 and 1464 cm^{-1} for C=O, C=N, C=C and C-N absorptions, respectively. In the IR spectra of compound **3**, the absorption peaks were observed at 3696 cm^{-1} for the O-H stretch and at 2995 and 2863 cm^{-1} for the aliphatic C-H stretch, while the peaks at 1764 and 1650 cm^{-1} belong to the C=O stretching vibrations. Peaks were observed at 1605 and 1481 cm^{-1} for the C=C and C-N stretching vibrations. The ^1H NMR spectrum confirmed the incorporation of the dicyclohexyl amine into the compound with signals at δ 1.97 (4H), 1.73 (4H), 1.25 (2H) and 1.09 (2H) ppm. This was confirmed in the ^{13}C NMR spectrum at δ 30.3, 25.6 and 24.6 ppm. The IR spectrum of compound **4** indicated the presence of a characteristic peak at 2981 cm^{-1} for the aliphatic C-H stretch, a peak at 1735 cm^{-1} for the C=O stretch, and a band at 1608 cm^{-1} due to C=N. The C=C stretch peaks are found at 1585 and 1565 cm^{-1} . Peaks were observed at 1483 and 1456 cm^{-1} for the C-N stretch. In the ^1H NMR spectrum, the absence of the aldehydic proton confirmed the formation of the imine. A signal was observed at δ 12.83 ppm for the hydroxyl group. Signals for aromatic protons were observed between δ 8.54 and 6.98 ppm. In the ^{13}C NMR spectrum, a signal was observed at δ 164.4 ppm for C=N, while signals were observed between δ 60.7 to 117.1 ppm for aromatic carbons. In the IR spectrum of compound **5**, the peak appearing at 2714 cm^{-1} is assigned to the C-H stretch, while the absorption peaks at 1612, 1561, and 1464 cm^{-1} are for the C=N, C=C and C-N vibrations, respectively. The ^1H NMR spectrum showed a signal for the hydroxyl group at δ 13.12 ppm, signals for aromatic protons were observed between δ 9.01 and 7.01

ppm. The IR spectrum of compound **6** showed the presence of an absorption peak at 3120 cm^{-1} for the O-H stretch and a peak at 2999 cm^{-1} for the C-H stretch. Peaks were observed at 1624 and 1599 cm^{-1} for the C=N and C=C, respectively. Although peaks were observed at 1465 and 1402 cm^{-1} for the CN stretch. A signal was observed at δ 13.12 ppm for the hydroxyl group in the ^1H NMR spectrum. Signals for aromatic protons were observed between δ 9.02 and 7.01 ppm. The ^{13}C NMR spectrum showed a signal at δ 165.1 ppm for (C=N) and signals for aromatic carbons were observed between δ 161.0 and 117.2 ppm. The IR spectrum of compound **7** showed the presence of absorption peaks at 2964, 1549, and 1363 cm^{-1} attributed to the stretches C-H, C=C, and C-O, respectively. A signal was observed at δ 13.32 ppm for the hydroxyl group in the ^1H NMR spectrum, while aromatic protons were observed between δ 8.93 and 6.97 ppm. In ^{13}C NMR, a signal was observed at δ 161.7 ppm for C=N, confirming the formation of imine. Aromatic signals lie between δ 160.7 and 115.1 ppm.

3.3. Crystal structure analysis

Compound **2** was recrystallized as white crystals from DMSO:toluene (1:1). The compound crystallizes in the space group C_2/c with eight molecules in the unit cell characterized by the unit cell parameters $a = 16.654(15)$ Å, $b = 8.789(7)$ Å, $c = 18.460(18)$ Å, $\beta = 102.89(5)^\circ$. The ORTEP diagram for compound **2** is presented in Figure 1. The crystallographic data and selected bond lengths and bond angles for compound **2** are provided in Tables 1-2. Whilst Table 3 gives the hydrogen bonding geometry of compound **2**.

The bond distances O21-C11, O21-C20, and O22-C20 are 1.386(2), 1.373(2), and 1.214(2) Å, respectively, are consistent with carbonyls [33], while the bond distances of N1-C19, N1-C32 and N1-C36 were 1.339(2), 1.465(3) and 1.457(2) Å, respectively, are consistent with the length of the C-N single bond [34]. The bond angles of C11-O21-C20, N1-C36-C35, and C19-N1-C32 were 122.1(1), 111.1(1) and 120.6(1) $^\circ$, respectively.

The coumarin ring is nearly coplanar with carbonyl oxygen displaced slightly above the plane of the ring. This coplanarity appears to be a general phenomenon observed in other compounds, even with more substitutions on the coumarin rings, including natural products [35]. The dihedral angle C11-O21-C20-O22 is $-176.25(14)^\circ$. The amide carbonyl linking the piperidine ring to the coumarin is, however, twisted out of the plane of the coumarin ring with the dihedral angle C36-N1-C19-C18 being $-4.4(2)^\circ$. Also the piperidine adopts a chair conformation with Cremer-Pople puckering parameters [36] $Q_2 = 0.547(2)$ Å and $\phi_2 = 167(7)^\circ$.

The eight molecules in the unit cell have been divided into two groups related by a two-fold symmetry. Each of the four molecules in each group can be further subdivided into two inner molecules and two outer molecules and are held together by non-classical C-H...O hydrogen bonds of varying lengths (Figure 2 and Table 3). The twist of the amide carbonyl out of the plane of the coumarin ring enables it to form bifurcated C-H...O contacts involving C4-H of the coumarin rings (C17-H according to the numbering scheme in Figure 1) of the two molecules sitting opposite to each other in the inner part of the network and an axial proton on the piperidine ring (C32-H) of another molecule that is perpendicular to it on the outer part of the network. The carbonyl of the coumarin moiety also engages the C14-H of another molecule in a C-H...O contact that completes the network. This arrangement results in coumarin rings of two outer molecules flanking the opposite sides of an inward-pointing piperidine ring of the inner molecules in a manner similar to open butterfly wings (Figure 2).

Table 1. Crystal data and details of the structure refinement for compound 2.

Empirical formula	C ₁₅ H ₁₅ NO ₃
Formula weight (g/mol)	257.28
Temperature (K)	296(2)
Crystal system	Monoclinic
Space group	C ₂ /c
a, (Å)	16.654(15)
b, (Å)	8.789(7)
c, (Å)	18.460(18)
β (°)	102.89(5)
Volume (Å ³)	2634(4)
Z	8
ρ _{calc} (g/cm ³)	1.298
μ (mm ⁻¹)	0.091
F(000)	1088.0
Crystal size (mm ³)	0.382 × 0.382 × 0.214
Radiation	MoKα (λ = 0.71073)
2θ range for data collection (°)	4.528 to 57.446
Index ranges	-21 ≤ h ≤ 22, -11 ≤ k ≤ 11, -24 ≤ l ≤ 24
Reflections collected	17626
Independent reflections	3321 [R _{int} = 0.0313, R _{sigma} = 0.0257]
Data/restraints/parameters	3321/0/172
Goodness-of-fit on F ²	1.047
Final R indexes [I ≥ 2σ (I)]	R ₁ = 0.0441, wR ₂ = 0.1134
Final R indexes [all data]	R ₁ = 0.0747, wR ₂ = 0.1329
Largest diff. peak/hole (e.Å ⁻³)	0.23/-0.17

Table 2. Summary of theoretical and experimental bond lengths (Å), and bond angles (°) for 3-[piperidine-1-carbonyl]-2H-chromen-2-one using B3LYP, CAM-B3LYP, B3PW91, wB97XD, and M06 functionals and 6-311G(d,p) basis set.

Bond lengths (Å)	Experimental	Theoretical					Minimum Deviation	Maximum Deviation
	XRD	B3LYP	CAM-B3LYP	B3PW91	wB97XD	M06		
O21-C11	1.386(2)	1.362	1.359	1.356	1.357	1.353	0.024	0.033
O21-C20	1.373(2)	1.396	1.380	1.389	1.377	1.383	0.04	0.023
O22-C20	1.214(2)	1.202	1.197	1.201	1.198	1.196	0.001	0.006
O23-C19	1.229(2)	1.225	1.220	1.223	1.219	1.217	0.006	0.012
N1-C19	1.339(2)	1.362	1.355	1.358	1.355	1.359	0.019	0.023
N1-C32	1.465(3)	1.467	1.460	1.459	1.458	1.456	0.002	0.009
N1-C36	1.457(2)	1.464	1.458	1.456	1.456	1.454	0.001	0.007
C11-C12	1.396(2)	1.404	1.394	1.403	1.396	1.397	0.001	0.008
C11-C16	1.381(3)	1.393	1.388	1.392	1.391	1.388	0.007	0.012
C12-C13	1.405(3)	1.407	1.400	1.404	1.401	1.400	0.001	0.005
C12-C17	1.430(2)	1.434	1.435	1.431	1.438	1.429	0.001	0.008
C13-C14	1.373(3)	1.384	1.378	1.382	1.380	1.378	0.005	0.011
C14-C15	1.386(3)	1.402	1.397	1.399	1.390	1.396	0.004	0.016
C15-C16	1.384(3)	1.388	1.381	1.386	1.383	1.382	0.001	0.004
C18-C19	1.505(2)	1.515	1.510	1.510	1.510	1.505	0.005	0.01
C18-C20	1.462(2)	1.466	1.466	1.462	1.467	1.461	0.001	0.005
C32-C33	1.510(3)	1.533	1.526	1.527	1.527	1.521	0.011	0.023
C33-C34	1.514(3)	1.535	1.528	1.529	1.530	1.522	0.008	0.021
Bond angles (°)	Experimental	Theoretical					Minimum Deviation	Maximum Deviation
	XRD	B3LYP	CAM-B3LYP	B3PW91	wB97XD	M06		
N1-C32-C33	111.1(2)	110.4	110.2	110.4	110.1	109.9	0.7	1.2
C11-O21-C20	122.1(1)	123.5	123.5	123.5	123.3	123.7	1.2	1.7
N1-C36-C35	111.1(1)	111.0	110.8	111.0	110.9	110.9	0.1	0.3
C19-N1-C32	120.6(1)	119.0	119.0	119.0	119.3	119.1	1.3	1.6
C19-N1-C36	125.4(1)	126.0	126.1	125.9	126.1	126.2	0.5	0.8
C32-N1-C36	114.0(1)	114.5	114.4	114.6	114.5	114.2	0.2	0.6
O21-C11-C12	121.2(1)	120.9	120.0	121.0	121.2	121.0	0.2	1.2
O21-C11-C16	117.1(2)	117.8	117.6	117.7	117.5	117.7	0.4	0.7
C12-C13-C14	120.1(2)	120.5	120.4	120.4	120.4	120.4	0.3	0.4
O23-C19-N1	123.3(1)	123.1	123.1	123.3	123.5	123.3	0.0	0.2
O23-C19-C18	117.6(1)	117.9	117.9	118.1	118.4	118.4	0.3	0.8
N1-C19-C18	119.1(1)	118.9	119.0	118.5	118.0	118.3	0.2	1.1
O21-C20-O22	116.6(1)	117.1	117.5	117.2	117.6	117.5	0.5	1.0
O21-C20-C18	117.1(1)	116.1	116.2	116.1	116.3	115.9	0.8	1.2
O22-C20-C18	126.3(2)	126.9	126.3	126.7	126.0	126.7	0.3	0.6

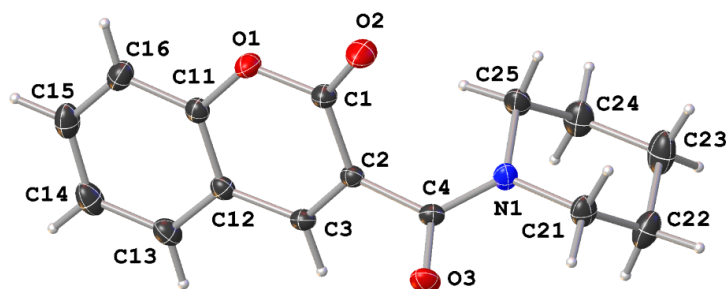
**Figure 1.** ORTEP view of 3-[piperidine-1-carbonyl]-2H-chromen-2-one (2) showing 50% probability displacement ellipsoids and atom labelling.

Table 3. Hydrogen-bond geometry for compound 2.

Donor-H...Acceptor *	D-H, Å	H...A, Å	D...A, Å	∠D-H...A, °
C3-H3...O3 ⁱ	0.93	2.36	3.246(4)	160
C14-H14...O2 ⁱⁱ	0.93	2.55	3.428(4)	158
C21-H21A...O3	0.97	2.35	2.767(3)	105

* Symmetry codes: *i* = -x, y, 1/2-z, *ii* = -1/2+x, -1/(2)y, z.

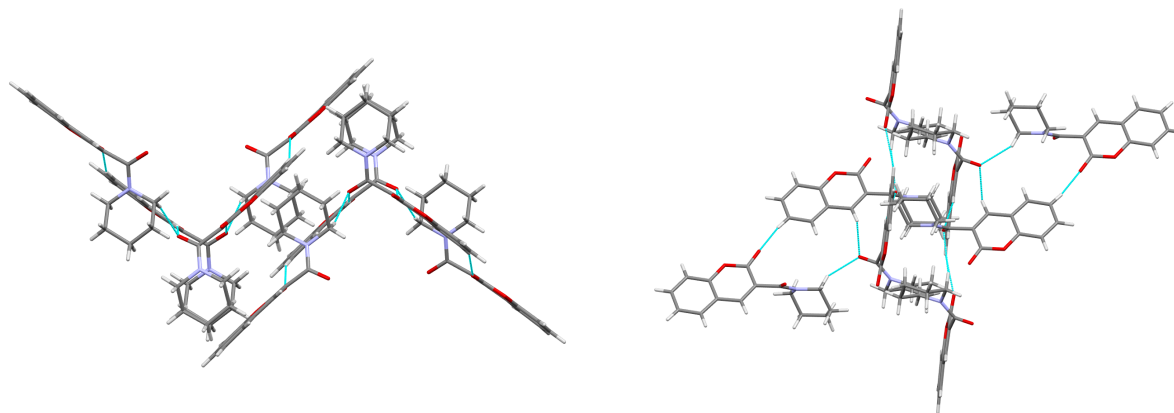


Figure 2. Crystal structure packing of the molecules in a unit cell of compound 2. Hydrogen bonding and contacts are shown as dashed lines.

3.4. Comparison of theoretical and experimental bond parameters for compound 2

Table 2 shows the summary of the theoretical and experimental bond lengths and bond angles for compound 2 using B3LYP, CAM-B3LYP, B3PW91, wB97XD and M06 functionals and 6-311G(d,p) basis set [37]. The functionals were chosen based on the computational results. The level of theory reported in the literature gave results that were consistent with the experimental results [38]. The bond lengths O21-C11, O21-C20, O22-C20, and O23-C19 for compound 2 were experimentally determined as 1.386(2), 1.373(2), 1.214(2) and 1.229(2) Å, respectively, while the calculated bond lengths gave deviations between 0.001 and 0.033 Å from the experimental values. The lengths of the bonds of the amide bonds N1-C19, N1-C32, and N1-C36 for compound 2 were experimentally determined as 1.339(2), 1.465(3) and 1.457(2) Å, respectively, while the calculated values deviated by 0.001-0.023 Å from the experimental values.

The crystallographically determined bond lengths of C11-C12, C11-C16, C12-C13, and C12-C17 were found at 1.396(2), 1.381(3), 1.405(3) and 1.430(2) Å while the calculated values gave deviations between 0.001 and 0.012 Å. The bond lengths of C13-C14, C14-C15, C15-C16, C18-C19 and C18-C20 were experimentally determined as 1.373(3), 1.386(3), 1.384(3), 1.505(2) and 1.462(2) Å with deviations between 0.001 and 0.016 Å representing the lowest and largest deviations, respectively, from the experimental values. The bond angles of C19-N1-C32, C19-N1-C36, and C32-N1-C36 were experimentally found to be 120.6(1), 125.4(1) and 114.0(1)°, whilst the computed values gave deviations of between 0.2 and 1.6° from the experimental values. Crystal data revealed that bond angles N1-C32-C33, N1-C36-C35, and N1-C19-C18 which were 111.1(2), 111.1(1) and 119.1(1)°, respectively, deviated from computed values by 0.1-1.2°. The bond angles of O21-C11-C12, O21-C11-C16, O23-C19-N1 and O23-C19-C18 were experimentally determined as 121.2(1), 117.1(2), 123.3(1) and 117.6(1)° whilst the computed values gave deviations of between 0.2 and 1.2° from the experimental values. The different functionals gave varying levels of agreement with the experimental results. But B3PW91 gave the computed values closest to the experimental values. The bond angles of O21-C20-O22, O21-C20-C18, and O22-C20-C18 were experimentally determined as 116.6(1), 117.1(1) and 126.3(2)° with deviations between 0.3 and 1.2° for the calculated values.

3.5. Hirshfeld surface analysis

Hirshfeld surface analysis is a quantitative way of studying the intermolecular interactions of molecules in a crystal structure. It gives details of their crystal packing behavior. Hirshfeld surface and fingerprint plots were mapped with Crystal Explorer 3.1 software [39]. The analysis was visualized by the normalized contact distance (d_{norm}), which was obtained using a high surface resolution with a static color scale, and computed with the equation below.

$$d_{\text{norm}} = \frac{d_i - r_{i\text{vdw}}}{r_{i\text{vdw}}} + \frac{d_e - r_{e\text{vdw}}}{r_{e\text{vdw}}} \quad (1)$$

In the equation, d_e is the distance from the Hirshfeld surface to the closest nucleus outside the surface, d_i is the corresponding distance to the nearest nucleus inside the surface, while r_{vdw} is the van der Waals radius of the atom [40]. The surface with a red, white, and blue color scheme describes the parameter d_{norm} [41]. The bright red spots denote the intermolecular contacts that are less than their vdW radii, while the blue spots indicate intermolecular contacts that are longer than their vdW radii. The white spots are the sum of their vdW radii.

Molecular Hirshfeld surfaces comprising d_{norm} surface, shape index, and curvedness of compound 2 were generated using a standard (high) surface resolution and are illustrated in Figure 3. The d_{norm} surface was mapped in the range of -0.2989 to 1.4342 Å, while d_i was mapped in the range of 0.9416 to 2.5552 Å. The parameter d_e was in the range of 0.9423 to 2.4959 Å, the shape index ranging from -1.0000 to 1.0000 Å and curvature lying between -4.0000 to 0.4000 Å.

Figure 4 shows the two-dimensional (2D) fingerprint plots from the Hirshfeld surface analysis of title compound 2. It illustrates the relative contribution (in percentage) of the major intermolecular contacts associated with it. The 2D fingerprint plots complement the Hirshfeld surface by providing quantitative information on the nature and type of intermolecular contacts [42-47]. The most important interaction is H-H, which contributes 48.3% to the overall crystal packing. Furthermore, the C-H (15.1%) and O-H (31.7%) fingerprint plots also provide information about the intermolecular hydrogen bonds and the contribution of the individual elements toward the crystal packing. The H-H interaction (indicated by one spike) is one of the most significant contacts. The fingerprint plot of the C-H contacts shows characteristic 'wings' that are identified as a result of weak C-H...π interactions.

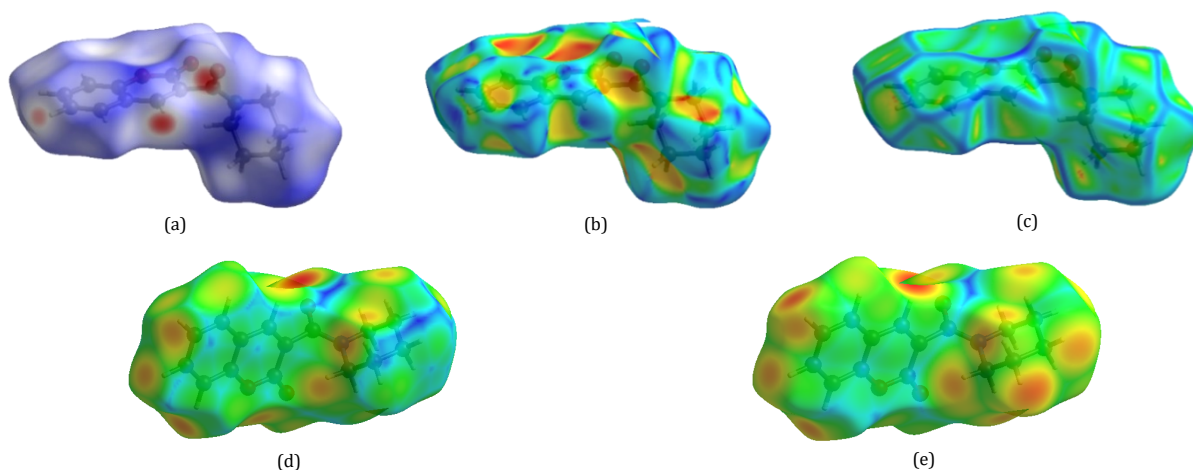


Figure 3. Hirshfeld surfaces mapped for (a) d_{norm} surface, (b) shape index, and (c) curvature, (d) d_e and (e) d_i of compound 2.

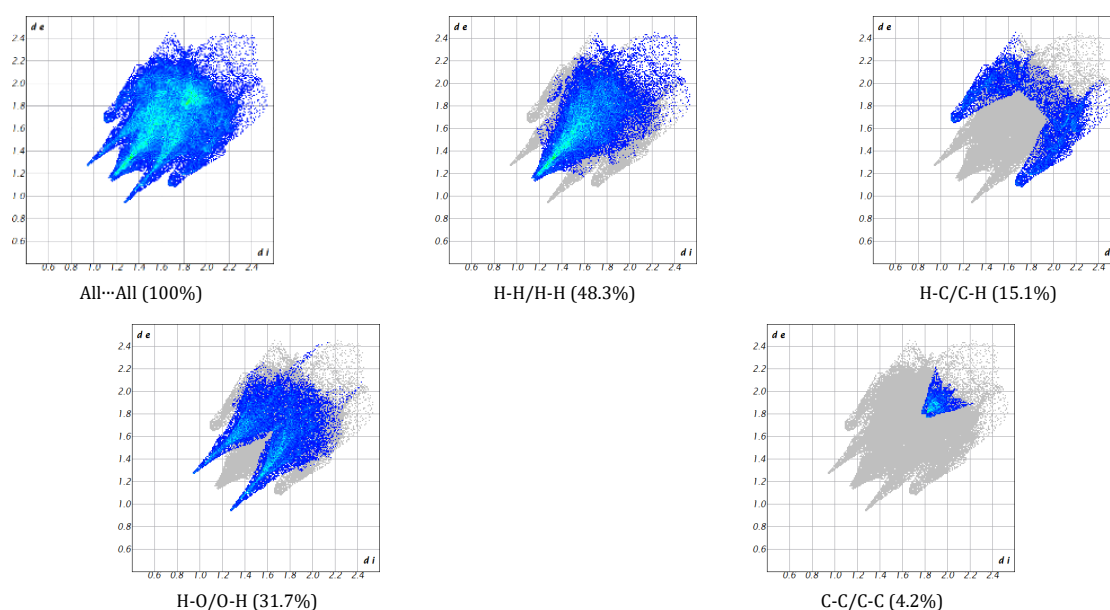


Figure 4. Relative contributions to the percentage of Hirshfeld surface area for various intermolecular contacts in 3-[piperidine-1-carbonyl]-2H-chromen-2-one.

The red triangles on the shape index represented by concave regions indicate π -stacking interactions, while the blue triangles represented by convex regions indicate the ring atoms of the molecule inside the surface. Curvedness indicates the electron density of surface curves around the molecular interactions. The flat areas of the surface correspond to a low value of curvedness, whereas a sharp curvature area corresponds to high values of curvedness and usually tends to divide the surface into patches, indicating contact between neighboring molecules. A large flat region delineated by a blue outline refers to π - π stacking interactions. In this compound, the curvedness suggests the absence of π - π stacking interactions [48-52]. The red spot is located over the oxygen that links the coumarin ring and the cyclic amine, which could be attributable to hydrogen bonding. And the π - π interaction of the terminal aromatic protons with neighboring molecules.

3.6. Chemical reactivity

E_{HOMO} and E_{LUMO} are the determinants of the chemical stability of any species [53]. The E_{HOMO} is associated with the ability to donate an electron while the E_{LUMO} is associated with

the ability to accept an electron. The energy of the HOMO determines the ionization potential, whilst the energy of the E_{LUMO} determines the electron affinity. The energy difference between the E_{HOMO} and E_{LUMO} orbitals, known as the energy gap, determines the stability or reactivity of molecules [54]. The energy gap also determines the electrical conductivity of the compound [55]. The lower the energy gap, the higher the conductivity, and *vice versa*. The hardness of a molecule also corresponds to the gap between the E_{HOMO} and E_{LUMO} orbitals [56].

The energy gap ($E_{HOMO}-E_{LUMO}$) is an important stability index used to characterize the chemical reactivity and kinetic stability of the molecule [57]. A molecule with a small energy gap is more polarized and reactive because it easily offers electrons to an acceptor. Low energy gap values may be due to conjugation [58]. The energies of the frontier molecular orbitals, the energy band gap ($E_{HOMO}-E_{LUMO}$), electronegativity (χ), chemical potential (μ), global hardness (η), global softness (S) and global electrophilicity index (ω) all contribute to the reactivity of the molecule concerned. The stability of the molecule is found to be related to hardness [59]. Electronegativity is the power of an atom in a molecule to attract an electron to itself.

Table 4. HOMO–LUMO energy levels of **2** using B3LYP, CAM-B3LYP, B3PW91, wB97XD and M06 functionals and 6-311G(d,p) basis set.

Energy levels (eV)	B3LYP	CAM-B3LYP	B3PW91	wB97XD	M06
LUMO+4	0.03593	0.07763	0.04550	0.11454	0.03216
LUMO+3	0.01276	0.06561	0.01357	0.09121	0.02020
LUMO+2	-0.01496	0.03680	-0.01583	0.05915	-0.00839
LUMO+1	-0.02852	0.02002	-0.02989	0.04221	-0.02335
LUMO	-0.08515	-0.03917	-0.08667	0.01604	-0.07958
HOMO	-0.24135	-0.29762	-0.24274	-0.31610	-0.25758
HOMO-1	-0.24426	-0.29819	-0.24596	-0.31784	-0.25814
HOMO-2	-0.26130	-0.31819	-0.26355	-0.33788	-0.27552
HOMO-3	-0.27394	-0.33127	-0.27675	-0.35083	-0.28737
HOMO-4	-0.29344	-0.35853	-0.29419	-0.37633	-0.31052
HOMO-LUMO gap	0.15620	0.25845	0.15607	0.33250	0.17790

Table 5. Summary of global reactivity descriptors for 3-[piperidine-1-carbonyl]-2H-chromen-2-one (**2**) using B3LYP, CAM-B3LYP, B3PW91, WB97XD and M06 functionals and the 6-311G(d,p) basis set.

Global reactivity descriptor	B3LYP	CAM-B3LYP	B3PW91	WB97XD	M06
Electronegativity (χ)	0.16325	0.33679	0.164705	0.30006	0.33716
Chemical potential (μ)	-0.16325	-0.33679	-0.164705	-0.30006	-0.33716
Global hardness (η)	0.15620	0.25845	0.156070	0.33214	0.17800
Global softness (S)	0.07810	0.12923	0.078035	0.16607	0.08900
Global electrophilicity index (ω)	0.00416	0.00733	0.002117	0.01495	0.01011

The electrophilicity index measures the reduction of energy due to the highest electron transfer between the donor and acceptor [60]. The electrophilicity is a descriptor of reactivity that allows a quantitative classification of the global electrophilic nature of a molecule within a relative scale. The new quantity of reactivity can be demonstrated to understand the toxicity of various pollutants in terms of their reactivity and site selectivity [61]. The HOMO-LUMO energy levels of compound **2** which were computed using B3LYP, CAM-B3LYP, B3PW91, wB97XD and M06 functionals, and the 6-311G(d,p) basis set is given in Table 4. E_{HOMO} and E_{LUMO} for compound **2** gave energy gaps between 0.1562 and 0.33520 eV for the different functionals and basis sets. The high energy gap is consistent with its high melting point and low solubility in most solvents [62].

Table 5 gives a summary of global reactivity descriptors for 3-[piperidine-1-carbonyl]-2H-chromen-2-one (**2**) using B3LYP, CAM-B3LYP, B3PW91, WB97XD and M06 functionals and 6-311G(d,p) basis set. The B3LYP functional gave the lowest electronegativity while the M06 functional gave the highest electronegativity, which confirms the limited scope of the B3LYP functional to capture all electron contributions in compound **2**. The reverse is observed in the computation of the chemical potential, which is highest for the B3LYP and lowest for the M06 functional. The WB97XD functional gave the highest value for global hardness while B3LYP gave the lowest value, and the same trend was observed in the computation of global softness. The B3PW91 functional gave the lowest global electrophilicity index, while the WB97XD gave the highest electrophilicity index.

4. Conclusion

Three new 2H-chromen-2-one and four known imine derivatives have been synthesised and characterised using FTIR, NMR, GC-MS, and microanalysis. The single crystal X-ray structure of 3-[piperidine-1-carbonyl]-2H-chromen-2-one (**2**) showed that the compound crystallised in the monoclinic space group C_2/c with eight molecules in the unit cell held together by a non-classical hydrogen bonding network. The Hirshfeld surface analysis has been presented to provide quantitative information on the nature and type of intermolecular contacts. The HOMO-LUMO gap of compound **2** is quite high, ranging from 0.1562 to 0.33520 eV depending on the functional used. This is consistent with the high stability of the compound.

Acknowledgements

The authors acknowledge the Centre for High Performance Computing in South Africa for the use of their computing resources (CHEM1261).

Supporting information

CCDC-2181456 contains the additional crystallographic data for this paper. These data can be obtained free of charge via <https://www.ccdc.cam.ac.uk/structures/>, or by e-mailing data_request@ccdc.cam.ac.uk, or by contacting The Cambridge Crystallographic Data Centre, 12 Union Road, Cambridge CB2 1EZ, UK; fax: +44(0)1223-336033.

Disclosure statement

Conflict of interest: The authors declare that they have no conflict of interest. Ethical approval: All ethical guidelines have been adhered to. Sample availability: Samples of the compounds are available from the author.

CRedit authorship contribution statement

Conceptualization: Felix Odame; Methodology: Felix Odame; Software: Eric Hosten, Jerry Joe Ebo Kingsley Harrison, Felix Odame; Validation: Eric Hosten, Jerry Joe Ebo Kingsley Harrison, Felix Odame; Formal Analysis: Eric Hosten, Jerry Joe Ebo Kingsley Harrison, Felix Odame; Investigation: Felix Odame, Tatenda Madanhire; Resources: Felix Odame; Data Curation: Felix Odame; Writing - Original Draft: Felix Odame; Writing - Review and Editing: Felix Odame, Tatenda Madanhire, Jerry Joe Ebo Kingsley Harrison, Nathaniel Owusu Boadi; Visualization: Felix Odame; Supervision: Felix Odame; Project Administration: Felix Odame.

ORCID and Email

Felix Odame

 felixessah15@gmail.com

 <https://orcid.org/0000-0001-7651-8816>

Tatenda Madanhire

 s210154810@mandela.ac.za

 <https://orcid.org/0000-0001-6352-183X>

Jerry Joe Ebo Kingsley Harrison

 jjharrison@ug.edu.gh

 <https://orcid.org/0000-0002-3153-3024>

Nathaniel Owusu Boadi

 noboadi@gmail.com

 <https://orcid.org/0000-0003-2673-7011>

Eric Hosten

 eric.hosten@mandela.ac.za

 <https://orcid.org/0000-0003-4173-2550>

References

- [1]. Abdel-Wahab, B. F.; Mohamed, H. A.; Farhat, A. A. Ethyl coumarin-3-carboxylate: Synthesis and chemical properties. *Org. Commun.* **2014**, *7*, 1-27 <https://acppubs.org/OC/2014/Volume%207/Issue%201/1-OC-1104-183.pdf>.
- [2]. Das, A. R.; Pal, G.; Bhattacharyya, P.; Ghosh, A. K.; Mukherjee, D.; Bandyopadhyay, D. Design and synthesis of coumarinyl 1,4-benzodioxanes as potential anti-oxidant. *Tetrahedron Lett.* **2012**, *53*, 7060-7066.
- [3]. Jumal, J.; Ayomide, A. F. Synthesis and radical scavenging activity of 6-hydroxyl-4-methylcoumarin and its derivatives. In *AIP Conference Proceedings*; AIP Conference Proceedings, 2018; pp. 1972, 030021, <https://doi.org/10.1063/1.5041242>.
- [4]. Al-Soud, Y. A.; Al-Sa'doni, H. H.; Amajaour, H. A. S.; Salih, K. S. M.; Mubarak, M. S.; Al-Masoudic, N. A. Synthesis, characterization and anti-HIV and antitumor activities of new coumarin derivatives. *Z. Naturforsch. B J. Chem. Sci.* **2008**, *63*, 83-89.
- [5]. Yilmaz, F. Microwave-assisted synthesis and biological evaluation of some coumarin hydrazides. *J. Turk. Chem. Soc. Sect. Chem.* **2018**, 551-568.
- [6]. Selvam, P.; Ramlakshmi, N.; Uma, G.; Arun Kumar, S.; Umamaheswari, A. Synthesis, characterisation and biological evaluation of novel coumarin derivatives. *Rasayan J. Chem.* **3**, 275-280, <http://www.rasayanjournal.co.in/vol-3/issue-2/14.pdf>.
- [7]. Rahman, F. S. A.; Yusufzai, S. K.; Osman, H.; Mohamad, D. Synthesis, characterisation and cytotoxicity activity of thiazole substitution of coumarin derivatives (characterisation of coumarin derivatives). *J. Phys. Sci.* **2016**, *27* (1), 77-87. <https://jps.usm.my/synthesis-characterisation-coumarin-derivatives/>
- [8]. Naik, C. G.; Malik, G. M.; Parekh, H. M. Novel coumarin derivatives: Synthesis, characterization and antimicrobial activity. *S. Afr. J. Chem.* **2019**, *72*, 248-252.
- [9]. García-Beltrán, O.; Yañez, O.; Caballero, J.; Galdámez, A.; Mena, N.; Nuñez, M. T.; Cassels, B. K. Synthesis of coumarin derivatives as fluorescent probes for membrane and cell dynamics studies. *Eur. J. Med. Chem.* **2014**, *76*, 79-86.
- [10]. Hafez, O. M. A.; Nassar, M. I.; El-Kousy, S. M.; Abdel-Razik, A. F.; Sherien, M. M. A.; El-Ghonemy, M. M. Synthesis of some new carbonitriles and pyrazole coumarin derivatives with potent antitumor and antimicrobial activities. *Acta Pol. Pharm.* **2014**, *71*, 594-601.
- [11]. Muthipeedika, N. J.; Bodke, Y. D.; Telkar, S.; Bakulev, V. A. Synthesis of coumarins linked with 1,2,3-triazoles under microwave irradiation and evaluation of their antimicrobial and antioxidant activity. *J. Mex. Chem. Soc.* **2019**, *64*, 53-73.
- [12]. Abduljabbar, T.; K. Hadi, M. Synthesis, characterization and antibacterial evaluation of some coumarin derivatives. *Iraqi J. Pharm. Sci.* **2021**, *30*, 249-257.
- [13]. Guan, A.-Y.; Liu, C.-L.; Li, M.; Li, Z.-N.; Zhang, M.-X.; Zhang, H. Synthesis and bioactivity of novel coumarin derivatives. *Nat. Prod. Commun.* **2011**, *6*, 1917-1920.
- [14]. Bensalah, D.; Mnasri, A.; Chakchouk-Mtibaa, A.; Mansour, L.; Mellouli, L.; Hamdi, N. Synthesis and antioxidant properties of some new thiazolyl coumarin derivatives. *Green Chem. Lett. Rev.* **2020**, *13*, 155-163.
- [15]. APEX2 (2010), SADABS and SAINT. Bruker AXS Inc., Madison, Wisconsin, USA.
- [16]. Sheldrick, G. M. A short history of SHELX. *Acta Crystallogr. A* **2008**, *64*, 112-122.
- [17]. Hübschle, C. B.; Sheldrick, G. M.; Dittrich, B. ShelXle: a Qt graphical user interface for SHELXL. *J. Appl. Crystallogr.* **2011**, *44*, 1281-1284.
- [18]. Odame, F.; Hosten, E.; Betz, R.; Lobb, K.; Tshentu, Z. Characterization and Computational Studies of 2-(Benzamido)Thiazol-5-yl Benzoate. *J. Struct. Chem.* **2019**, *60*, 136-142.
- [19]. Odame, F.; Hosten, E. C.; Lobb, K.; Tshentu, Z. Ultrasound promoted synthesis, characterization and computational studies of some thiourea derivatives. *J. Mol. Struct.* **2020**, *1216*, 128302.
- [20]. Odame, F.; Hosten, E. C.; Tshentu, Z. R. Synthesis, characterization, and computational studies of n-[(9e)-8,10,17-triazatetracyclo [8.7.0.0.2, 7.0.11, 16]heptadeca-1(17), 2, 4, 6, 11(16), 12, 14-heptaen-9-ylidene] benzamide. *J. Struct. Chem.* **2020**, *61*, 1177-1185.
- [21]. Farrugia, L. J. ORTEP-3 for Windows - a version of ORTEP-III with a Graphical User Interface (GUI). *J. Appl. Crystallogr.* **1997**, *30*, 565-565.
- [22]. Macrae, C. F.; Bruno, I. J.; Chisholm, J. A.; Edgington, P. R.; McCabe, P.; Pidcock, E.; Rodriguez-Monge, L.; Taylor, R.; van de Streek, J.; Wood, P. A. Mercury CSD 2.0- new features for the visualization and investigation of crystal structures. *J. Appl. Crystallogr.* **2008**, *41*, 466-470.
- [23]. Spek, A. L. Structure validation in chemical crystallography. *Acta Crystallogr. D Biol. Crystallogr.* **2009**, *65*, 148-155.
- [24]. Frisch, M. J.; Trucks, G. W.; Schlegel, H. B.; Scuseria, G. E.; Robb, M. A.; Cheeseman, J. R.; Montgomery, J. A.; Vreven, T.; Kudin, K. N.; Burant, J. C.; Millam, J. M.; Iyengar, S. S.; Tomasi, J.; Barone, V.; Mennucci, B.; Cossi, M.; Scalmani, G.; Rega, N.; Petersson, G. A.; Nakatsuji, H.; Hada, M.; Ehara, M.; Toyota, K.; Fukuda, R.; Hasegawa, J.; Ishida, M.; Nakajima, T.; Honda, Y.; Kitao, O.; Nakai, H.; Klene, M.; Li, X.; Knox, J. E.; Hratchian, H. P.; Cross, J. B.; Adamo, C.; Jaramillo, J.; Gomperts, R.; Stratmann, R. E.; Yazyev, O.; Austin, A. J.; Cammi, R.; Pomelli, C.; Ochterski, J. W.; Ayala, P. Y.; Morokuma, K.; Voth, G. A.; Salvador, P.; Dannenberg, J. J.; Zakrzewski, V. G.; Dapprich, S.; Daniels, A. D.; Strain, M. C.; Farkas, O.; Malick, D. K.; Rabuck, A. D.; Raghavachari, K.; Foresman, J. B.; Ortiz, J. V.; Cui, Q.; Baboul, A. G.; Clifford, S.; Cioslowski, J.; Stefanov, B. B.; Liu, G.; Liashenko, A.; Piskorz, P.; Komaromi, I.; Martin, R. L.; Fox, D. J.; Keith, T.; Al-Laham, M. A.; Peng, C. Y.; Nanayakkara, A.; Challacombe, M.; Gill, P. M. W.; Johnson, B.; Chen, W.; Wong, M. W.; Gonzalez, C.; Pople, J. A. Gaussian 09, Revision A.02, Gaussian, Inc., Wallingford CT, 2016.
- [25]. Salomon, O.; Reiher, M.; Hess, B. A. Assertion and validation of the performance of the B3LYP* functional for the first transition metal row and the G2 test set. *J. Chem. Phys.* **2002**, *117*, 4729-4737.
- [26]. Yanai, T.; Tew, D. P.; Handy, N. C. A new hybrid exchange-correlation functional using the Coulomb-attenuating method (CAM-B3LYP). *Chem. Phys. Lett.* **2004**, *393*, 51-57.
- [27]. Salavati-Niasari, M.; Mirsattari, S. N.; Monajjemi, M.; Hamadian, M. Density functional B3LYP and B3PW91 studies of the properties of four cyclic organodiboranes with tetramethylene fragments. *J. Struct. Chem.* **2010**, *51*, 437-443.
- [28]. Chai, J.-D.; Head-Gordon, M. Long-range corrected hybrid density functionals with damped atom-atom dispersion corrections. *Phys. Chem. Chem. Phys.* **2008**, *10*, 6615-6620.
- [29]. Zhao, Y.; Truhlar, D. G. The M06 suite of density functionals for main group thermochemistry, thermochemical kinetics, noncovalent interactions, excited states, and transition elements: two new functionals and systematic testing of four M06 functionals and 12 other functionals. *Theor. Chem. Acc.* **2008**, *119*, 525-525.
- [30]. Dunning, T. H., Jr Gaussian basis sets for use in correlated molecular calculations. I. The atoms boron through neon and hydrogen. *J. Chem. Phys.* **1989**, *90*, 1007-1023.
- [31]. Hanwell, M. D.; Curtis, D. E.; Lonie, D. C.; Vandermeersch, T.; Zurek, E.; Hutchison, G. R. Avogadro: an advanced semantic chemical editor, visualization, and analysis platform. *J. Cheminform.* **2012**, *4*, 17.
- [32]. GaussView, Version 6, Dennington, Roy; Keith, Todd A.; Millam, John M. Semichem Inc., Shawnee Mission, KS, 2016.
- [33]. Odame, F.; Schoeman, R.; Krause, J.; Hosten, E. C.; Tshentu, Z. R.; Frost, C. Synthesis, characterization, crystal structures, and anticancer activity of some new 2,3-dihydro-1,5-benzoxazepines. *Med. Chem. Res.* **2021**, *30*, 987-1004.
- [34]. Odame, F.; Hosten, E. C.; Betz, R.; Krause, J.; Frost, C. L.; Lobb, K.; Tshentu, Z. R. Synthesis, characterization, computational studies and DPPH scavenging activity of some triazatetracyclic derivatives. *J. Iran. Chem. Soc.* **2021**, *18*, 1979-1995.
- [35]. Harrison, J. J. E. K.; Ayine-Tora, M. D.; Appiagyei, B.; Mills-Robertson, F. C.; Asomaning, W. A.; Achel, D. G.; Ishida, H.; Kingsford-Adaboh, R. Crystal structure and in vitro antimicrobial activity studies of Robustic acid and other Alpinumisoflavones isolated from *Milletia thonningii*. *Z. Kristallogr. Cryst. Mater.* **2019**, *234*, 229-235.
- [36]. Cremer, D.; Pople, J. A. General definition of ring puckering coordinates. *J. Am. Chem. Soc.* **1975**, *97*, 1354-1358.
- [37]. Al-Hazmy, S. M.; Zouaghi, M. O.; Al-Johani, J. N.; Arfaoui, Y.; Al-Ashwal, R.; Hammami, B.; Alhagri, I. A.; Alhemiary, N. A.; Hamdi, N. Chemosensing properties of coumarin derivatives: Promising agents with diverse pharmacological properties, docking and DFT investigation. *Molecules* **2022**, *27*.
- [38]. Mohammad, A.-T.; Al-Mohammed, M. H.; Ghdayeb, M. Z.; Husain Al-Majidi, S. M. Coumarin dimers of benzidine and phenylenediamine cores: synthesis, characterisation and mesomorphic properties. *Liq. Cryst.* **2020**, *47*, 414-422.
- [39]. Spackman, P. R.; Turner, M. J.; McKinnon, J. J.; Wolff, S. K.; Grimwood, D. J.; Jayatilaka, D.; Spackman, M. A. CrystalExplorer: a program for Hirshfeld surface analysis, visualization and quantitative analysis of molecular crystals. *J. Appl. Crystallogr.* **2021**, *54*, 1006-1011.
- [40]. Guin, M.; Khanna, S.; Elavarasi, S. B.; Sarkar, P. DFT calculations, Hirshfeld surface analysis and docking studies of 3-anisaldehyde thiosemicarbazone. *J. Chem. Sci. (Bangalore)* **2020**, *132*.
- [41]. Chandrasekaran, R.; Murugavel, S.; Guin, M.; Silambarasan, T. Crystal structure, Hirshfeld, computational biomolecular investigations, and MTT assay studies of amino pyrimidine derivative as EGFR kinase domain inhibitor. *J. Mol. Struct.* **2022**, *1254*, 132416.
- [42]. Munshi, S. J.; Guin, M.; Kundu, S.; Kumar, S. B. Synthesis, structures and Hirshfeld surface analysis of Ni(II) and Co(III) complexes with N2O donor Schiff base ligand. *J. Indian Chem. Soc.* **2021**, *98*, 100080.
- [43]. Kumar, S. B.; Munshi, S. J.; Sadhu, M. H.; Guin, M. Synthesis, structure and molecular Hirshfeld surface analysis of polymeric cadmium(II) complex involving tetradentate N3S-donor ligand and dicyanamide as bridging ligand. *Ind. J. Chem.* **2021**, *60*, 663-668.
- [44]. Guin, M.; Halder, S.; Chatterjee, S.; Konar, S. Synthesis, X-ray crystal structure of Cu(II) 1D coordination Polymer: In View of Hirshfeld surface, FMO, Molecular electrostatic potential (MEP) and Natural Bond orbital (NBO) analyses. *J. Mol. Struct.* **2022**, *1270*, 133949.

- [45]. Ramalingam, A.; Sambandam, S.; Medimagh, M.; Al-Dossary, O.; Issaoui, N.; Wojcik, M. J. Study of a new piperidone as an anti-Alzheimer agent: Molecular docking, electronic and intermolecular interaction investigations by DFT method. *J. King Saud Univ. Sci.* **2021**, *33*, 101632.
- [46]. Arulraj, R. Hirshfeld surface analysis, interaction energy calculation and spectroscopic study of 3-chloro-3-methyl-r(2),c(6)-bis(p-tolyl)piperidin-4-one using DFT approaches. *J. Mol. Struct.* **2022**, *1248*, 131483.
- [47]. Dhandapani, A.; Veeramankandan, S.; Kumar, R. S.; Almansour, A. I.; Arumugam, N.; Subashchandrabose, S.; Suresh, J.; Arulraj, R.; Gajalakshmi, D. Synthesis, in vitro and in silico antitumor evaluation of 3-(2,6-dichlorophenyl)-1,5-diphenylpentane-1,5-dione: Structure, spectroscopic, RDG, Hirshfeld and DFT based analyses. *J. Mol. Struct.* **2022**, *1251*, 132002.
- [48]. Ramalingam, A.; Kansız, S.; Dege, N.; Sambandam, S. Synthesis, crystal structure, DFT calculations and Hirshfeld surface analysis of 3-chloro-2,6-bis(4-chlorophenyl)-3-methylpiperidin-4-one. *J. Chem. Crystallogr.* **2021**, *51*, 273–287.
- [49]. Kumar, A.; Sambandam, S.; Ramalingam, A.; Krishnamoorthy, R.; Arumugam, D.; Oyenyin, O. E. Synthesis, molecular docking of 3-(2-chloroethyl)-2,6-diphenylpiperidin-4-one: Hirshfeld surface, spectroscopic and DFT based analyses. *J. Mol. Struct.* **2022**, *1262*, 132993.
- [50]. Arulraj, R.; Sivakumar, S.; Suresh, S.; Anitha, K. Synthesis, vibrational spectra, DFT calculations, Hirshfeld surface analysis and molecular docking study of 3-chloro-3-methyl-2,6-diphenylpiperidin-4-one. *Spectrochim. Acta A Mol. Biomol. Spectrosc.* **2020**, *232*, 118166.
- [51]. Arulraj, R.; Sivakumar, S.; Rajkumar, K.; Jasinski, J. P.; Kaur, M.; Thiruvalluvar, A. Synthesis, Crystal Structure, DFT Calculations and Hirshfeld Surface Analysis of 3-Chloro-3-methyl-r(2),c(6)-bis(p-methoxyphenyl)piperidin-4-one. *J. Chem. Crystallogr.* **2020**, *50*, 41–51.
- [52]. Ashfaq, M.; Munawar, K. S.; Bogdanov, G.; Ali, A.; Tahir, M. N.; Ahmed, G.; Ramalingam, A.; Alam, M. M.; Imran, M.; Sambandam, S.; Munir, B. Single crystal inspection, Hirshfeld surface investigation and DFT study of a novel derivative of 4-fluoroaniline: 4-((4-fluorophenyl)amino)-4-oxobutanoic acid (BFAOB). *J. Iran. Chem. Soc.* **2022**, *19*, 1953–1961.
- [53]. Poiyamozi, A.; Sundaraganesan, N.; Karabacak, M.; Tanriverdi, O.; Kurt, M. The spectroscopic (FTIR, FT-Raman, UV and NMR), first-order hyperpolarizability and HOMO–LUMO analysis of 4-amino-5-chloro-2-methoxybenzoic acid. *J. Mol. Struct.* **2012**, *1024*, 1–12.
- [54]. Udhayakala, P.; Jayanthi A.; Rajendiran, T. V.; Gunasekarand S. Molecular structure, FT-IR and FT-Raman spectra and HOMO-LUMO analysis of 2-methoxy-4-nitroaniline using ab initio HF and DFT (B3LYP/B3PW91) calculations. *Archives of Applied Science Research* **2011**, *3*, 424–439, <http://www.scholarsresearchlibrary.com/aasr-vol3-iss4/AASR-2011-3-4-424-439.pdf>.
- [55]. Govindarajan, M.; Perianthy, S.; Carthigayen, K. FT-IR and FT-Raman spectra, thermo dynamical behavior, HOMO and LUMO, UV, NLO properties, computed frequency estimation analysis and electronic structure calculations on α -bromotoluene. *Spectrochim. Acta A Mol. Biomol. Spectrosc.* **2012**, *97*, 411–422.
- [56]. Murugavel S.; Manikandan, N.; Lakshmanan, D.; Naveen, K.; Perumal, P. T. Synthesis, crystal structure, DFT and antibacterial activity studies of (E)-2-benzyl-3-(furan-3-yl)-6,7-dimethoxy-4-(2-phenyl-1H-inden-1-ylidene)-1,2,3,4-tetrahydroisoquinoline. *J. Chil. Chem. Soc.* **2015**, *60*(3), 3015–3020.
- [57]. Parr, R. G.; Chattaraj, P. K. Principle of maximum hardness. *J. Am. Chem. Soc.* **1991**, *113*, 1854–1855.
- [58]. Pauling, L. *The nature of the chemical bond: An introduction to modern structural chemistry*; 3rd ed.; Cornell University Press: Ithaca, NY, 1960.
- [59]. Parr, R. G.; Szentpály, L. v.; Liu, S. Electrophilicity index. *J. Am. Chem. Soc.* **1999**, *121*, 1922–1924.
- [60]. Parthasarathi, R.; Padmanabhan, J.; Subramanian, V.; Maiti, B.; Chattaraj, P. K. Chemical reactivity profiles of two selected polychlorinated biphenyls. *J. Phys. Chem. A* **2003**, *107*, 10346–10352.
- [61]. Parthasarathi, R.; Subramanian, V.; Roy, D. R.; Chattaraj, P. K. Electrophilicity index as a possible descriptor of biological activity. *Bioorg. Med. Chem.* **2004**, *12*, 5533–5543.
- [62]. Aihara, J.-I. Reduced HOMO–LUMO gap as an index of kinetic stability for polycyclic aromatic hydrocarbons. *J. Phys. Chem. A* **1999**, *103*, 7487–7495.



Copyright © 2023 by Authors. This work is published and licensed by Atlanta Publishing House LLC, Atlanta, GA, USA. The full terms of this license are available at <http://www.eurjchem.com/index.php/eurjchem/pages/view/terms> and incorporate the Creative Commons Attribution-Non Commercial (CC BY NC) (International, v4.0) License (<http://creativecommons.org/licenses/by-nc/4.0>). By accessing the work, you hereby accept the Terms. This is an open access article distributed under the terms and conditions of the CC BY NC License, which permits unrestricted non-commercial use, distribution, and reproduction in any medium, provided the original work is properly cited without any further permission from Atlanta Publishing House LLC (European Journal of Chemistry). No use, distribution, or reproduction is permitted which does not comply with these terms. Permissions for commercial use of this work beyond the scope of the License (<http://www.eurjchem.com/index.php/eurjchem/pages/view/terms>) are administered by Atlanta Publishing House LLC (European Journal of Chemistry).